Research Article Vol. 57, No. 19 / 1 July 2018 / Applied Optics 5443

applied optics

Quantitative estimation of elemental composition employing a synthetic generated spectrum

Prashant Kumar,[1] Rajesh K. Kushawaha,[1] S. B. Banerjee,[1] K. P. Subramanian,[1,*] and N. G. Rudraswami[2]

[1]Physical Research Laboratory, Ahmedabad, India
[2]National Institute of Oceanography, Dona Paula, India
*Corresponding author: subba@prl.res.in

Received 1 March 2018; revised 18 May 2018; accepted 1 June 2018; posted 4 June 2018 (Doc. ID 325238); published 28 June 2018

Composition of multielement samples is estimated by using a synthetic generated spectrum utilizing a nonlinear fitting routine. By fitting simultaneously a large number of emission lines, the error in the estimation is minimized. The procedure for synthetic spectrum generation includes self-absorption of emission lines by taking into account the number density of different species in the plasma. The Stark width of different emission lines is iteratively calculated based on the observed width and the degree of self-absorption in the individual lines. This procedure is found to be successful for achieving convergence of the retrieval algorithm even for dense spectra as well as for resolving merged lines with accuracy. This scheme was applied on a stainless steel and brass sample, and the laser-induced breakdown spectroscopy results match well with the reference value obtained from the electron probe microanalyzer measurement.

OCIS codes: (300.6360) Spectroscopy, laser; (300.6365) Spectroscopy, laser induced breakdown; (300.2140) Emission; (300.3700) Linewidth.

https://doi.org/10.1364/AO.57.005443

1. INTRODUCTION

Owing to the ease of its application to various scenarios, the calibration-free laser-induced breakdown spectroscopy (CF-LIBS) procedure has gained considerable importance in recent times [1–6]. The advantage of working without having a prior knowledge of the target enables the technique to be used for various cases such as planetary exploration [7], archeology [8], geology [9], forensic sciences [10], etc. The procedure is simple and, under certain plasma conditions, can be used to retrieve the elemental composition of samples under study. Most of the existing calibration-free procedures involve plasma temperature calculation using the Boltzmann plot method, assuming a local thermodynamic equilibrium (LTE) for the emitting species [6,11–14].

While the assumption of LTE is at the heart of the CF-LIBS procedure, the other major assumptions of optically thin plasma have been relaxed by accounting for self-absorption, using the curve of growth technique [15]. Under this procedure, the observed line intensities in the LIBS spectrum are corrected for different degrees of self-absorption. An alternate approach was demonstrated by Gornushkin *et al.* [16,17] through a post-breakdown model to predict number densities and plasma parameters at different times of evolution based on an initial input of these parameters. This radiation dynamic model assumes LTE for the same time after plasma initiation [18], and then the evolution of various parameters are obtained. Monte Carlo simulated annealing technique is then utilized to vary the initial assumption of the parameters to match the predicted results with the experimental spectrum. Though this method automatically incorporates the effect of self-absorption as well as spatial inhomogeneity in plasma, it suffers from a disadvantage that the Monte Carlo approach is time and resource consuming. Moreover, this post-breakdown model was found to give satisfactory results only up to few hundreds of nanoseconds from plasma formation. This technique, when compared with the conventional CF-LIBS method, was found to have more errors while estimating the concentration [19]. The large error is due to the fact that only a few emission lines could be simulated owing to huge computational time (several hours to days). In a recent work [20], it was shown that by using a larger computational facility (parallel computing on graphical processing unit), the analysis time could be brought down to a few seconds for a small number of emission lines. But again, the requirement of a huge computational facility reduces the applicability of this procedure. Another approach was suggested by Yaroshchyk *et al.* [21] and more recently by Gerhard *et al.* [22], which is based on evaluating spectral line intensities of different transitions using the classical theory of spectral radiance from LTE plasma and comparing it with

experimental spectrum. The work by Yaroshchyk *et al.* [21] brings out the importance of having an automated routine for analysis for minimizing human involvement starting from line identification to concentration estimation. But the scheme ignores self-absorption and Stark broadening for most of the emission lines and hence gives semiquantitative results, with large errors in concentration estimation. The work by Gerhard *et al.* [22] involves a proper selection of emission lines to avoid optically thick and merged lines from the analysis. Moreover, in both of the above works, only a limited number of emission lines are used for the analysis, which affects the results obtained for concentration values.

The present work relies on the previously reported procedures [15,16,20–22], of utilizing the technique of synthetically generated spectra to estimate the concentration from multielement samples. The major improvements include simultaneous fitting of plasma parameters on a large number of emission lines. The model does not make any approximation for optically thin plasma, and all plasma parameters, *viz.*, temperature, number densities of different species, width of the spectral lines, and concentration values, are obtained simultaneously. The model can easily be tuned to include factors affecting the line profile intensity such as instrument factor and spectrometer resolution. The effect of emission lines merging together in an actual experiment can also be handled rather easily here. A technique to perform an automated search of prominent emission lines of various species is also presented, which can be very useful while identifying lines for an unknown sample. With these improvements, two different alloys were analyzed to test the performance of this method.

2. THEORETICAL GENERATION OF LIBS SPECTRA

The model presented here is derived under the assumption of a homogeneous and collisionally averaged plasma in which, within a short acquisition time, any temporal variations are neglected. These assumptions would necessarily mean that the emission line profile or LIBS spectra for a sample under LTE conditions is determined mainly by five parameters, *viz.*, plasma temperature (T), electron number density (N_e), concentration (C), absorption path length (l_{abs}), and the instrument factor (F_{inst}). The equation for intensity of plasma emission line profile for any transition is given as [15,23]

$$I_{ji}(\lambda) = F_{\text{inst}} \frac{8\pi hc^2}{\lambda_0^5} \frac{n_j}{n_i} \frac{g_i}{g_j} (1 - e^{-\kappa(\lambda) l_{\text{abs}}}), \tag{1}$$

where, $I_{ji}(\lambda)$ is the intensity of emission line for a transition between an upper "j" level to a lower "i" level. λ_0 is the central wavelength of the transition, and n_i, n_j, g_i, and g_j are the number densities and statistical weights of the "i" and "j" levels. It may be noted that linearization of this general Eq. (1) reproduces the familiar LIBS equation. The absorption coefficient $\kappa(\lambda)$ is given by

$$\kappa(\lambda) = \kappa_0 \frac{a}{\pi} \int_{-\infty}^{+\infty} \frac{e^{-t^2}}{(t - x)^2 + a^2} \, \mathrm{d}t, \tag{2}$$

where κ_0 is given as

$$\kappa_0 = \frac{2e_c^2 \pi^{\frac{1}{2}} \sqrt{ln2}}{mc^2} f_{ij} n_i \frac{\lambda^2}{\Delta\lambda_G}, \tag{3}$$

where e_c is the electronic charge. The Voigt integral in Eq. (2) gives the emission line profile, which depends on both Lorentzian and Gaussian widths. The terms a and x in that equation are given by

$$a = \frac{\Delta\lambda_L}{\Delta\lambda_G} \sqrt{ln2}, \tag{4}$$

$$x = 2\sqrt{ln2} \frac{\lambda - \lambda_0}{\Delta\lambda_G}. \tag{5}$$

In the above equations, f_{ij} is the oscillator strength of the particular transition, and $\Delta\lambda_L$ and $\Delta\lambda_G$ are the Lorentzian and Gaussian widths (full width at half-maximum [FWHM]) of the emission line profile. While the atomic parameters for the transitions are available at NIST [24] and Kurucz [25] databases, $\Delta\lambda_L$ and $\Delta\lambda_G$ of the emission lines are in turn dependent upon the plasma parameters, *viz.*, electron number density and temperature. The absorption path length (l_{abs}) is assumed to be constant over a short acquisition time and is typically of the order of centimeters for a LIBS plasma in vacuum [26]. The major contributors to the Lorentzian width ($\Delta\lambda_L$) are the broadening due to Stark effect and natural lifetime, while the Gaussian component comprises the Doppler broadening due to thermal motion of the emitting species. It may be noted that the recorded profile in the experiment is a convolution of the instrumental response function and emission line profile as given in Eq. (1).

Assuming a Boltzmann distribution, population of any level "k" with energy E_k and degeneracy g_k can be written in terms of the total number density n_0 of that species as

$$n_k = \frac{n_0 g_k}{U(T)} e^{\frac{-E_k}{k_B T}}, \tag{6}$$

where $U(T)$ is the partition function of the emitting species at temperature T. Using the above Eq. (6), the intensity Eq. (1) and the opacity Eq. (3) can then be written as

$$I_{ji}(\lambda) = F_{\text{inst}} \frac{8\pi hc^2}{\lambda_0^5} e^{-\frac{E_j - E_i}{k_B T}} (1 - e^{-\kappa(\lambda) l_{\text{abs}}}), \tag{7}$$

$$\kappa_0 = \frac{2e_c^2 \pi^{\frac{1}{2}} \sqrt{ln2}}{mc^2} f_{ij} \frac{n_0 g_i}{U(T)} e^{\frac{-E_i}{k_B T}} \frac{\lambda^2}{\Delta\lambda_G}. \tag{8}$$

In order to generate a LIBS spectra theoretically, the inputs required can be classified under three categories:

- Global parameters: constants for all of the emission lines, namely, F_{inst}, T, and l_{abs}.
- Semi-local parameters: constants for emission line of a particular plasma species, $U(T)$ and n_0.
- Local parameters: atomic transition constants and line widths for individual lines, g_i, g_j, E_i, E_j, f_{ij}, λ_0, $\Delta\lambda_G$, and $\Delta\lambda_L$.

The semi-local parameters, $U(T)$ and n_0, can be obtained, once we have the value of temperature, concentration, and electron number density. Except for the Stark effect contribution to the Lorentzian broadening, all other local parameters for the transition are either available or can be derived from the

plasma parameters. To generate the synthetic LIBS spectra, we assume a constant value for the parameters l_{abs} and $\Delta\omega_L(=|\frac{c}{\lambda^2}|\Delta\lambda_L)$ for each of the emission lines. It may be noted that the assumption of a constant value for these parameters is made only for the theoretical generation of a LIBS spectra. When this model is fitted to a LIBS spectra, the value $\Delta\lambda_L$ can be obtained as a result of fitting.

The estimation of the total number density of a particular emitting species, n_0 from T, electron number density N_e, and concentration C, is not straightforward and is obtained through an iterative procedure involving simultaneous agreement of the Saha ionization equation and plasma neutrality condition. The algorithm to obtain this value is shown in Fig. 1.

The procedure starts with given values of T, N_e, and C as inputs. The concentration C is a matrix containing individual concentration values for each element denoted by c_i's such that,

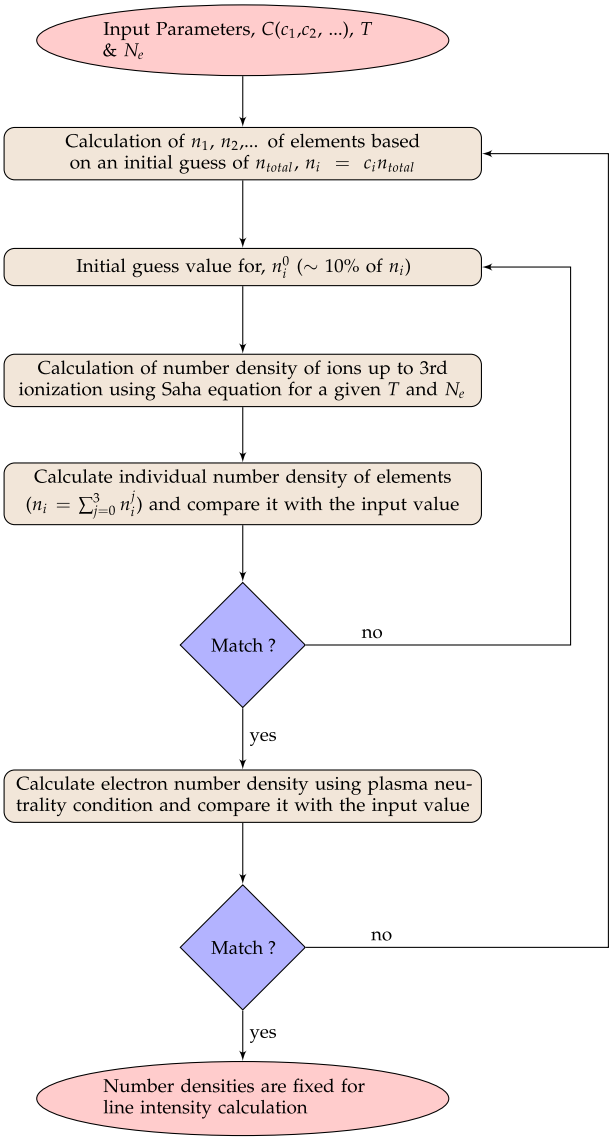

Fig. 1. Algorithm to calculate number density of individual species from N_e, T, and C.

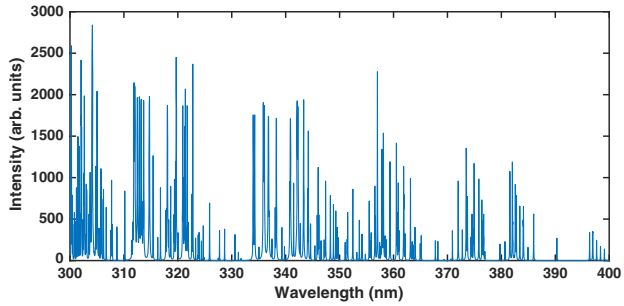

Fig. 2. Synthetic generated spectra for steel [Fe(70%), Cr(20%), Mn(2%), Ni(8%)] at 12,000 K and $N_e = 5 \times 10^{16}$ cm^{-3} assuming an absorption length of 2 cm and same Lorentzian width, $\Delta\omega_L$ for the spectral lines.

$$C = [c_1\ c_2\ c_3 \ldots c_n], \tag{9}$$

$$\sum_{i=0}^{i=n} c_i = 1. \tag{10}$$

An initial value of total number density (n_{total}) is assumed, and using concentration value (C), the number density for each of the individual elements (n_1, n_2,...) is obtained by $n_i = c_i n_{\text{total}}$. From the number density of each element (n_i's), a guess value of neutral number densities (n_i^0) are assumed (~10% of total number density). Using the Saha equation, number densities of ionic components for each element are estimated, and their sum is compared with the assumed value of the number density of respective elements. This section is iterated until an agreement is achieved between the input number density of each element and the calculated value. Once they agree within a set tolerance value, the next step is to calculate value of N_e using the obtained ionic number density by applying the plasma neutrality condition, which is then compared with input value of N_e. If the input and the calculated value match, the number densities are fixed and are passed on to the model for calculating the intensity using Eq. (1). If they do not match, the assumed value of total number density is iterated until a convergence is achieved.

To evaluate the Voigt integral mentioned in Eq. (2), a method that uses Fourier expansion of the complex error function [27] has been used. A theoretically generated spectra for a steel sample with composition as Fe 70%, Cr 20%, Mn 2%, and Ni 8% using the above model at a temperature $T = 12,000$ K and $N_e = 5 \times 10^{16}$ cm^{-3} is shown in Fig. 2. This spectrum is fitted onto the measured LIBS spectrum, and species concentrations are estimated.

The above model, which can synthetically generate a LIBS spectra for a multi-element sample, will be of immense help in understanding the expected accuracy in concentration estimation and limit of detection in the CF-LIBS procedure due to various errors. These errors can be experimental or errors in data for atomic transition constants.

3. LINE PROFILE FITTING ROUTINE

The fitting routine utilizes the above model to obtain various parameters from a given LIBS spectrum. The model is passed as a function to a nonlinear least square fitting routine to fit the

input spectra. The output parameters of the fitting routine are the plasma temperature, electron number density, instrument factor, and number densities (and hence concentration) of all the identified species. The uncertainty in the value of absorption length, l_{abs} and F_{inst}, is removed by using the normalization procedure. The value of $\Delta\lambda_L$ to be used as an input parameter is obtained iteratively by applying proper corrections to the observed widths due to self-absorption. This procedure and other steps towards realization of an automated fitting routine are presented below.

A. Automated Search Procedure

Unambiguous identification of an emission line in the LIBS spectra is of utmost importance to derive a reliable estimate of the concentration. For the multi-element sample, correct identification and labeling is challenging due to the presence of multiple lines in the vicinity. Even for a single element, multiple transitions having almost the same central wavelength are possible. Though the wavelength may match for multiple lines, the strength of a particular transition depends on various factors. Hence, to correctly identify an emission line, we propose a simple technique. From an exhaustive database of atomic transitions for a given species, a comprehensive sub-list is made in which the wavelength of transitions of various species are sorted based on their prominence under LTE condition at 1 eV. For this, the formula of peak intensity for an optically thin plasma under LTE is used,

$$I_{ji}^{\text{peak}} = \alpha \frac{g_i f}{\lambda_0^3} e^{\frac{-E_j}{k_B T(=1\,\text{eV})}}, \tag{11}$$

where α is a constant that contains the total number density and partition function of a particular species. A table of transitions sorted by their respective strengths can then be prepared using the above equation for each species. A temperature value of 1 eV in the above equation is only a typical value used to search for the prominent emission lines at that temperature. It should be noted that it has no bearing to the actual plasma temperature, which is obtained as a result of fitting. The search procedure starts with selecting a small number of transitions for each species having maximum strength fetched from the sub-list mentioned above. It is then used to label corresponding transitions in the LIBS spectrum. The number of transitions in the search procedure is gradually increased so that most of the emission lines in the LIBS spectra are accounted for. This procedure has been very useful in identifying and labeling the emission lines obtained in the steel and brass spectra.

B. Estimation of Partition Function

Since the procedure for line profile fitting involves iteration of multi-parameters, $U(T)$, being a function of estimated temperature, needs to updated at each step of iteration. The calculation of the partition function involves the sum over all the energy states for a particular species. This is quite cumbersome, and a simple solution to this issue is to obtain the value of $U(T)$ at any T using interpolation on a predetermined database. This is created using $U(T)$ values obtained for different species from NIST database [24] at temperatures from 0.5 to 1.5 eV in steps of 0.05 eV. Usually, the LIBS plasma is well within this temperature regime.

C. Normalization to Account for l_{abs} and Instrument Factor, F_{inst}

From ionic lines present in the LIBS spectrum, the model also estimates the value of electron number density. It can be seen from Eqs. (1) and (3) that the total absorption by plasma is directly proportional to the product of n_0 and l_{abs}. If only first-order terms are considered while expanding the exponential term in Eq. (1), we observe that line intensity is proportional to the product of F_{inst}, n_0, and l_{abs}. This introduces the problem that the individual values cannot be determined simultaneously through iteration. This needs to be resolved prior to the calculation of the final concentrations. This is done by using the plasma neutrality condition, which is used for normalization of the number density. Note that the electron number density calculation from the Saha equation does not suffer from this problem because the ratios of number densities involved in the equation cancels these unknown constants. While the value of F_{inst} is obtained as a result of the fitting routine, we need to constrain the value of l_{abs}. For this, the fitting is performed starting from a few millimeters to a few centimeters, which is considered as a reasonable bound for the plasma absorption length [26]. The error introduced by uncertainty in this parameter is incorporated in the final concentration estimate.

D. Estimation of Input $\Delta\lambda_L$ to the Model

As discussed in the previous section, the Lorentzian width is mainly due to Stark broadening of the emission lines. The observed emission line widths depend on both the Lorentzian width as well as on the broadening due to self-absorption. Hence, a direct estimate of the Stark widths through Voigt profile fitting of the observed emission lines poses a problem. To resolve this, the following approach was followed. The first step was to evaluate the error in the concentration and other plasma parameters when observed Lorentzian width is used as an input to the model. For this, a synthetic spectrum of brass was generated assuming $T = 14{,}000$ K and $N_e = 3 \times 10^{15}$ cm^{-3} for the optically thin case and $N_e = 3 \times 10^{16}$ cm^{-3} for the optically thick case. The value of $\Delta\lambda_L$ was arbitrarily generated between 0.01 to 0.16 nm for the set of emission lines. To check the accuracy of the procedure, a simultaneous fitting was performed on the set of lines for the optically thin case. The fitted values obtained for $\Delta\lambda_L$ showed reasonably good agreement with the input values, as can be seen from Fig. 3, for the optically thin case. Other plasma parameters were also obtained and are shown in Table 1.

Thereafter, the fitting was performed for the $N_e = 3 \times 10^{16}$ case, for which some of the lines showed broadening due to self-absorption. For this case, we have directly used the observed line width as an input to the model. While there is large error in the value of $\Delta\lambda_L$ obtained from fitting and the input values (Fig. 3), the concentration values show only a slight difference, (Table 1). The next step is to correct for the values of $\Delta\lambda_L$, which was done using the method presented in [15], by defining a self-absorption parameter (SA). This parameter can be used to relate the observed width of the line with its true width. The method has been successfully demonstrated by Bredice *et al.* [28] to evaluate the Stark broadening parameter of a few Mn lines. Mathematically, this parameter is given by

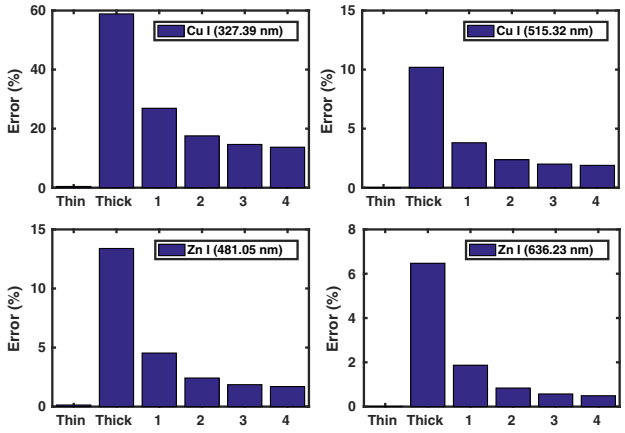

Fig. 3. Error in $\Delta\lambda_L$ obtained after fitting for thin and thick plasma conditions. Note the change in error values after subsequent corrections applied at each iteration (numbers 1–4 shown in the plot). Only a few lines are shown in order to demonstrate this iterative correction scheme.

Table 1. Plasma Parameters Obtained Using Fitting Routine at Different Iterations Performed for Correction of the Observed Line Width[a]

Parameter	T (in K)	$N_e(\times 10^{15}$ cm$^{-3})$	C (in %)
Thin	14046	3.16	[55.91; 44.09]
Thick	13876	25.8	[55.49; 44.51]
Iter 1	13959	28.5	[55.69; 44.31]
Iter 2	13979	29.2	[55.74; 44.26]
Iter 3	13985	29.4	[55.75; 44.25]
Iter 4	13987	29.5	[55.76; 44.24]

[a]The input values are $T = 14{,}000$ K, $N_e = 3 \times 10^{15}$ cm^{-3} for thin and $N_e = 3 \times 10^{16}$ cm^{-3} for thick plasma condition. The composition of brass used to generate the synthetic spectra is [Cu (56%); Zn (44%)].

$$\mathrm{SA} = \frac{I_{\mathrm{obs}}}{I_{\mathrm{thin}}}, \tag{12}$$

where I_{obs} is the observed intensity obtained for thick plasma, and I_{thin} is the intensity considering plasma to be optically thin. A value of I_{thin}, and hence SA, was calculated for each fitting cycle. The $\Delta\lambda_L$ values were then corrected for its true value using the relation mentioned in [15,28],

$$\Delta\lambda_{\mathrm{obs}} = \frac{\Delta\lambda_{\mathrm{true}}}{\sqrt{\mathrm{SA}}}. \tag{13}$$

The corrected values obtained from the previous relation are then passed on to the routine for the next iteration cycle. The results obtained for error in the calculated value of $\Delta\lambda_L$ at each step of calculation for a few sets of lines is shown in Fig. 3. The plasma parameters obtained at different iterations are also shown in Table 1.

Hence, the above technique was found to give a reasonably good estimate of true $\Delta\lambda_L$ using iterative corrections to observed values using the SA.

The fitting procedure is completely automated, and all above algorithms and procedures are incorporated in different MATLAB sub routines. Before using the above line profile fitting routine on actual experimental spectra, it was tested on the synthetically generated spectra. Output parameters perfectly matched with the input parameters used to generate the LIBS spectra. The iterative procedure starts with an initial temperature value of 10,000 K and electron number density value of 10^{16} cm^{-3}. The complete automated routine takes about 20–30 min of computing time on a standard PC to retrieve all the parameters from the input spectrum.

4. EXPERIMENTAL SETUP

A schematic of the experimental setup is shown in Fig. 4. The experimental system consisted of an Nd:YAG laser (Innolas Spitlight 600) operated at its fundamental wavelength (1064 nm). The pulse energy used in the experiment was ~400 mJ with laser pulse duration of 6 ns. The laser was focused onto the target placed inside a vacuum chamber with base pressure of 10^{-2} mbar. The lens has a focal length of 30 cm, and the spot size on the target was ~500 μm, which gives a power density of $\sim 3.4 \times 10^{10}$ W/cm^2. The emission from the plasma is collected using a collecting optics (Andor CC52) and is focused onto the optical fiber, which is fed to an echelle spectrometer (Andor Mechelle 5000) coupled with a gated ICCD camera (Andor iStar DH334T).

Steel and brass samples were used in the experiment. To compare the results from the LIBS analysis, a reference value of the concentration was obtained by performing electron probe microanalyzer (EPMA) measurements on the same samples. An overview of this analytical technique is presented in the Ref. [29]. The EPMA measurements were performed at National Institute of Oceanography, Goa. The acquisition delay and gate width used for recording the spectra were 400 and 400 ns, respectively. The timing of various triggers in the experiment was controlled and monitored using a fast digital oscilloscope (Keysight InfiniiVision). The delay was sufficient to suppress the continuum and to get a good signal-to-noise ratio. The spectra for both the samples were recorded in the wavelength region of 300–700 nm and were averaged over 500 shots for better repeatability. To avoid pitting of the sample, the target was moved after every 20 shots using XY translation stage inside the vacuum chamber.

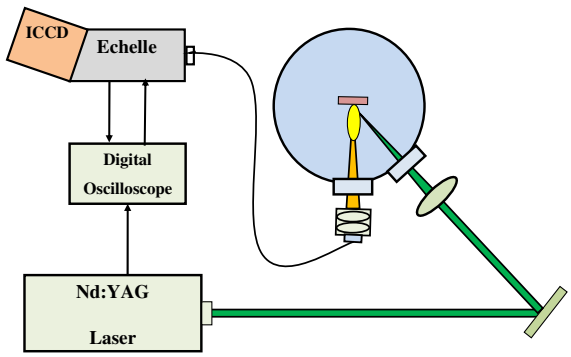

Fig. 4. Schematic of the experimental system used for recording LIBS spectra of steel and brass sample.

5. ANALYSIS AND RESULTS

A. Wavelength and Intensity Calibration

The wavelength calibration in the above wavelength region was performed using a standard Hg–Ar source (Ocean Optics HG-1). For intensity calibration, a deuterium halogen source (Ocean Optics DH-3 plus) was used. The band spectrum recorded using this source was smoothed by applying the Savitzky–Golay algorithm (MATLAB in-built library), which was then used to obtain correction factors for the final intensity. Transmission characteristics of all optical components (quartz viewport, collecting optics) used in the experiment were estimated and used for calibration of intensity. Background subtraction was also performed before correcting the intensity. Calibrated spectra of the steel and brass sample are shown in Fig. 5.

B. Line Identification

The automatic search procedure mentioned in the previous section was employed to construct a set of prominent transitions for various species in the plasma. The input database to this procedure consisted of over 13,000 lines for steel (Fe I, Fe II, Cr I, Cr II, Mn I, Mn II, Ni I, and Ni II) and 1600 lines for brass (Cu I, Cu II and Zn I), out of which 190 prominent lines were selected for steel and 56 lines for the brass sample. Hence, we could correctly identify and label almost all of the detected emission lines above a set threshold. A list of the selected lines used for generating the synthetic spectrum are shown in Table 2 for the brass sample and Table 3 for the steel sample.

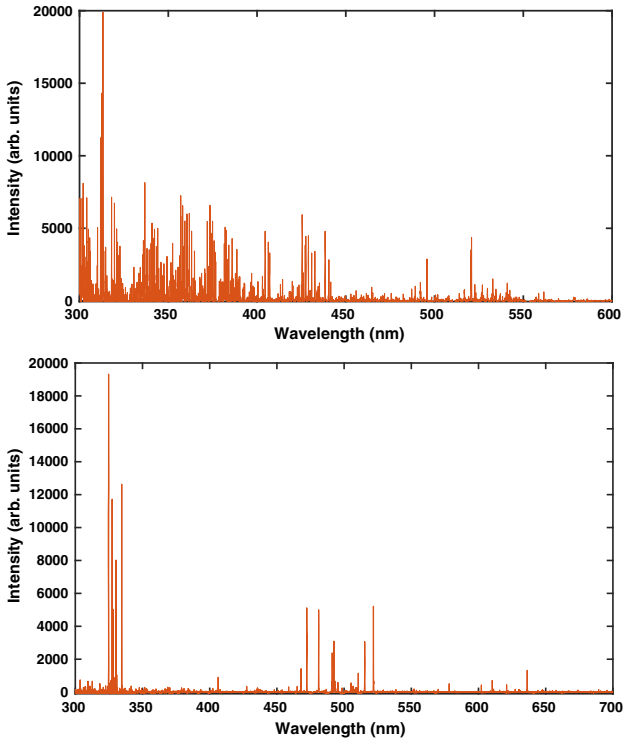

Fig. 5. Calibrated LIBS spectrum obtained for (top) steel and (bottom) brass sample.

Table 2. List of Emission Lines Used for the Synthetic Spectrum Generation for Brass (Cu, Zn) Sample[a]

Cu I	324.31	327.39	327.98	329.05	330.79	331.72
	331.96	333.78	334.92	336.53	341.4	347.6
	351.18	352.42	352.74	353.38	368.74	402.26
	406.26	427.51	437.81	450.93	453.08	453.97
	458.69	465.11	467.48	470.45	510.55	515.32
	521.82	522.01	529.25	578.21		
Cu II	490.97	491.79	493.16	493.72	495.16	495.37
	500.68	502.12	504.73	505.18	506.54	506.7
	508.82	621.69	627.33			
Zn I	328.23	330.26	334.5	468.01	472.22	481.05
	636.23					

[a]The wavelength values are expressed in nm.

Table 3. List of Emission Lines Used for the Synthetic Spectrum Generation for Steel (Fe, Cr, Mn, Ni) Sample[a]

Fe I	300.09	300.81	300.96	302.58	303.74	304.76
	305.9	306.72	307.57	319.69	320.04	321.16
	321.96	322.58	323.94	328.67	330.6	340.75
	342.71	344.06	346.58	347.54	349.06	353.66
	354.1	354.2	355.5	355.85	356.54	357.02
	358.12	358.53	358.61	358.7	360.54	360.67
	360.88	361.02	361.88	362.14	363.14	364.04
	365.14	368.74	370.92	371.99	372.76	373.48
	373.71	374.34	374.56	374.82	374.94	375.82
	376.38	376.56	376.72	379.5	381.58	382.04
	382.12	382.58	382.78	383.42	384.04	384.1
	385.99	388.62	390.29	396.92	404.58	406.35
	407.17	414.38	426.04	427.17	430.79	432.58
	438.35	440.48				
Fe II	300.26	306.22	307.72	313.54	315.42	316.78
	317.75	318.31	318.67	319.29	319.38	319.6
	321.04	321.34	325.9			
Cr I	300.5	301.37	301.48	301.76	301.84	302.06
	302.43	303.02	303.42	303.98	304.08	305.38
	323.77	343.36	357.43	358.43	359.34	360.53
	363.66	363.98	384.94	385.89	396.36	397.66
	398.38	399.11	425.43	427.48	428.97	520.45
	520.6	520.84				
Cr II	302.66	305.01	312.26	312.5	312.86	313.2
	313.66	314.72	315.22	318.06	320.92	321.74
	333.98	334.26	334.78	336.02	337.83	337.94
	337.98	338.26	339.14	339.3	340.24	
Mn I	323.68	324.85	353.19	354.78	382.35	403.08
	403.3	403.44	403.57	404.14	404.87	445.16
	476.23	478.34	482.35			
Mn II	346.03	347.4				
Ni I	300.36	301.19	303.79	305.08	305.76	310.15
	323.29	336.96	338.06	341.48	344.62	345.84
	346.16	347.25	349.3	351.03	351.5	352.45
	356.64	361.94				
Ni II	308.7	347.14	351.39			

[a]The wavelength values are expressed in nm.

C. Results

The model described in the previous section was fitted onto the LIBS spectrum of both samples. Simultaneous fitting was performed on all of the identified lines. The final values

Table 4. Concentration Estimates for Steel and Brass Sample Obtained Using Proposed LIBS Technique Compared to the Reference Value Obtained Using EPMA[a]

Sample	Element	Present Work (LIBS)	Reference (EPMA)
Steel	Cr	17.81 ± 1.68	19.64 ± 0.29
	Fe	71.08 ± 3.24	69.62 ± 0.51
	Mn	2.92 ± 0.24	1.77 ± 0.22
	Ni	8.19 ± 1.31	8.96 ± 0.33
Brass	Cu	57.79 ± 1.24	59.48 ± 0.48
	Zn	42.21 ± 1.24	40.51 ± 0.46

[a]The range is specified based on a 95% confidence interval obtained from chi-square value of the estimated parameters (temperature and neutral number densities).

for the plasma parameters, *viz.*, temperature and electron number density, were $10,100 \pm 600$ K and $3.1 \pm 1.9 \times 10^{16}$ cm^{-3} in the case of the steel sample and $13,200 \pm 700$ K and $2.2 \pm 0.9 \times 10^{16}$ cm^{-3} for the brass sample. The concentration estimate obtained for both the samples is presented in Table 4 along with the values obtained using EPMA. A part of the fitted spectra overlaid on the experimental spectra is also shown in Figs. 6 and 7. The concentration values shown in Table 4 are the results obtained from the final iteration for the best fit to the experimental spectrum.

Some of the lines appearing in the experimental spectrum were not simulated due to the lack of availability of the atomic transition parameters for those lines. As mentioned earlier, the simulated spectra are obtained under an assumption of homogeneous LTE plasma and could be one of the reasons for the small mismatch with the experimental spectrum for some of the lines. Other sources of error in the simulated spectra could be the errors in the atomic transition constants, mostly the oscillator strengths of the lines and partition function of the emitting species. Though the results obtained from this method give a reliable estimate of concentration for major elements, the estimation of minor constituent is not precise. This can be understood in terms of the accumulated effect of errors in major elements and subsequent normalization of concentration, which results in larger errors for minor elements. Nevertheless, the advantage of using this method can easily be seen in Fig. 7 as to how closely it can match the experimental spectra even in the case where two lines are very nearby.

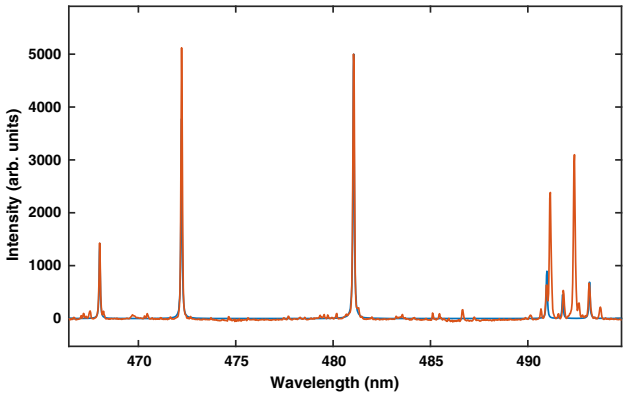

Fig. 6. Part of (blue curve) synthetic spectrum fitted on the (orange curve) experimentally derived LIBS spectra for brass sample.

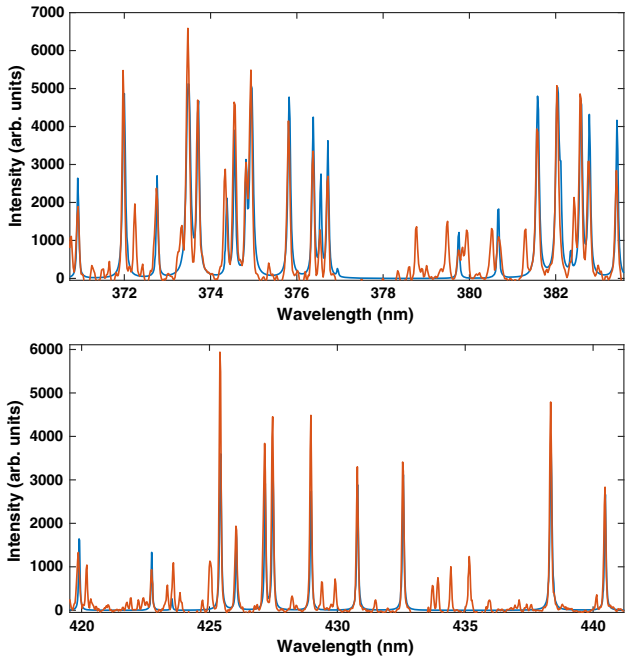

Fig. 7. Part of (blue curve) synthetic spectrum fitted on the (orange curve) experimentally derived LIBS spectra for steel sample.

6. CONCLUSION

An algorithm based on fitting synthetic generated spectra to experimental spectra has been demonstrated for estimating the elemental concentration in samples. The major improvement of this procedure as compared to previously reported works [19,21,22] employing a synthetic spectra scheme is the extended range of spectral coverage and hence improved accuracy. These improvements are made possible by the ability of the new scheme to handle a large number of lines appearing in a single LIBS spectrum. From the results shown in Table 4 and Figs. 6 and 7, it can be seen that the above procedure is quite successful in retrieving full plasma parameters from the LIBS spectra. It is also demonstrated that this method is capable of resolving the merged lines. These features enable this scheme of analysis applicable for a wide range of LIBS spectra collected for different samples under varied ambient conditions. The estimation of concentrations from the temperature value obtained using usual the Boltzmann plot is abandoned in this scheme, and is estimated by fitting the parameters directly.

Another improvement incorporated in the current procedure is the inclusion of the effect of self-absorption in the model, rather than applying a correction to the observed spectra. The self-absorption is correctly included in the linear regime of Beer–Lambert law without relying on any models. The Lorentzian widths due to Stark broadening for different lines are estimated by an iterative scheme using SA. The partition functions, which depend on temperature, are correctly accounted for in every iteration, to the most probable value, by interpolating the data set. Thus, the retrieval of elemental

concentration by fitting synthetic spectra onto LIBS spectra seems to be a robust scheme over a wide range of plasma formation, each satisfying the LTE conditions, and holds promise for further research in this direction.

Acknowledgment. The SEM/EPMA analyses is supported by Project Number PSC0106.

REFERENCES

1. J. D. Winefordner, I. B. Gornushkin, T. Correll, E. Gibb, B. W. Smith, and N. Omenetto, "Comparing several atomic spectrometric methods to the super stars: special emphasis on laser induced breakdown spectrometry, LIBS, a future super star," J. Anal. At. Spectrom. **19**, 1061–1083 (2004).
2. Q. Zeng, L. Guo, X. Li, M. Shen, Y. Zhu, J. Li, X. Yang, K. Li, J. Duan, X. Zeng, and Y. Lu, "Quantitative analyses of Mn, V, and Si elements in steels using a portable laser-induced breakdown spectroscopy system based on a fiber laser," J. Anal. At. Spectrom. **31**, 767–772 (2016).
3. B. Praher, V. Palleschi, R. Viskup, J. Heitz, and J. Pedarnig, "Calibration free laser-induced breakdown spectroscopy of oxide materials," Spectrochim. Acta B **65**, 671–679 (2010).
4. J. Xiu, S. Zhong, H. Hou, Y. Lu, and R. Zheng, "Quantitative determination of manganese in aqueous solutions and seawater by laser-induced breakdown spectroscopy (LIBS) using paper substrates," Appl. Spectrosc. **68**, 1039–1045 (2014).
5. E. M. Cahoon and J. R. Almirall, "Quantitative analysis of liquids from aerosols and microdrops using laser induced breakdown spectroscopy," Anal. Chem. **84**, 2239–2244 (2012).
6. F. de Oliveira Borges, J. U. Ospina, G. de Holanda Cavalcanti, E. E. Farias, A. A. Rocha, P. I. L. B. Ferreira, G. C. Gomes, and A. Mello, "CF-LIBS analysis of frozen aqueous solution samples by using a standard internal reference and correcting the self-absorption effect," J. Anal. At. Spectrom. **33**, 629–641 (2018).
7. F. Colao, R. Fantoni, V. Lazic, A. Paolini, F. Fabbri, G. Ori, L. Marinangeli, and A. Baliva, "Investigation of LIBS feasibility for in situ planetary exploration: an analysis on Martian rock analogues," Planet. Space Sci. **52**, 117–123 (2004).
8. A. Giakoumaki, K. Melessanaki, and D. Anglos, "Laser-induced breakdown spectroscopy (LIBS) in archaeological science—applications and prospects," Anal. Bioanal. Chem. **387**, 749–760 (2007).
9. R. S. Harmon, R. E. Russo, and R. R. Hark, "Applications of laser-induced breakdown spectroscopy for geochemical and environmental analysis: a comprehensive review," Spectrochim. Acta B **87**, 11–26 (2013).
10. C. M. Bridge, J. Powell, K. L. Steele, and M. E. Sigman, "Forensic comparative glass analysis by laser-induced breakdown spectroscopy," Spectrochim. Acta B **62**, 1419–1425 (2007).
11. A. Ciucci, M. Corsi, V. Palleschi, S. Rastelli, A. Salvetti, and E. Tognoni, "New procedure for quantitative elemental analysis by laser-induced plasma spectroscopy," Appl. Spectrosc. **53**, 960–964 (1999).
12. J. Gomba, C. D'Angelo, D. Bertuccelli, and G. Bertuccelli, "Spectroscopic characterization of laser induced breakdown in aluminium–lithium alloy samples for quantitative determination of traces," Spectrochim. Acta B **56**, 695–705 (2001).
13. P. Kumar, K. P. Subramanian, A. Kumar, and R. K. Singh, "Improved algorithm for elemental analysis by laser-induced breakdown spectroscopy," Appl. Opt. **52**, 5178–5183 (2013).
14. J. Aguilera and C. Aragón, "Multi-element Saha–Boltzmann and Boltzmann plots in laser-induced plasmas," Spectrochim. Acta B **62**, 378–385 (2007).
15. D. Bulajic, M. Corsi, G. Cristoforetti, S. Legnaioli, V. Palleschi, A. Salvetti, and E. Tognoni, "A procedure for correcting self-absorption in calibration free-laser induced breakdown spectroscopy," Spectrochim. Acta B **57**, 339–353 (2002).
16. I. Gornushkin, A. Kazakov, N. Omenetto, B. Smith, and J. Winefordner, "Radiation dynamics of post-breakdown laser induced plasma," Spectrochim. Acta B **59**, 401–418 (2004).
17. I. Gornushkin, A. Kazakov, N. Omenetto, B. Smith, and J. Winefordner, "Experimental verification of a radiative model of laser-induced plasma expanding into vacuum," Spectrochim. Acta B **60**, 215–230 (2005).
18. G. Cristoforetti, A. D. Giacomo, M. Dell'Aglio, S. Legnaioli, E. Tognoni, V. Palleschi, and N. Omenetto, "Local thermodynamic equilibrium in laser-induced breakdown spectroscopy: beyond the McWhirter criterion," Spectrochim. Acta B **65**, 86–95 (2010).
19. K. K. Herrera, E. Tognoni, I. B. Gornushkin, N. Omenetto, B. W. Smith, and J. D. Winefordner, "Comparative study of two standard-free approaches in laser-induced breakdown spectroscopy as applied to the quantitative analysis of aluminum alloy standards under vacuum conditions," J. Anal. At. Spectrom. **24**, 426–438 (2009).
20. A. Demidov, S. Eschlböck-Fuchs, A. Kazakov, I. Gornushkin, P. Kolmhofer, J. Pedarnig, N. Huber, J. Heitz, T. Schmid, R. Rössler, and U. Panne, "Monte Carlo standardless approach for laser induced breakdown spectroscopy based on massive parallel graphic processing unit computing," Spectrochim. Acta B **125**, 97–102 (2016).
21. P. Yaroshchyk, D. Body, R. J. Morrison, and B. L. Chadwick, "A semi-quantitative standard-less analysis method for laser-induced breakdown spectroscopy," Spectrochim. Acta B **61**, 200–209 (2006).
22. C. Gerhard, J. Hermann, L. Mercadier, L. Loewenthal, E. Axente, C. Luculescu, T. Sarnet, M. Sentis, and W. Viöl, "Quantitative analyses of glass via laser-induced breakdown spectroscopy in argon," Spectrochim. Acta B **101**, 32–45 (2014).
23. W. Lochte-Holtgreven, *Plasma Diagnostics* (North-Holland, 1968).
24. A. Kramida, Yu. Ralchenko, and J. Reader, and NIST ASD Team, "NIST atomic spectra database (ver. 5.3)," August 24, 2017, available at http://physics.nist.gov/asd [National Institute of Standards and Technology, Gaithersburg, Maryland (2015)].
25. R. Kurucz and B. Bell, "Atomic spectral line database from CD-ROM 23 of R. L. Kurucz," available at https://www.cfa.harvard.edu/amp/ampdata/kurucz23/sekur.html [Smithsonian Astrophysical Observatory (1995)].
26. R. K. Singh, A. Kumar, B. G. Patel, and K. P. Subramanian, "Role of ambient gas and laser fluence in governing the dynamics of the plasma plumes produced by laser blow off of LiF-C thin film," J. Appl. Phys. **101**, 103301 (2007).
27. S. Abrarov, B. Quine, and R. Jagpal, "Rapidly convergent series for high-accuracy calculation of the Voigt function," J. Quant. Spectrosc. Radiat. Transfer **111**, 372–375 (2010).
28. F. Bredice, F. Borges, H. Sobral, M. Villagran-Muniz, H. D. Rocco, G. Cristoforetti, S. Legnaioli, V. Palleschi, A. Salvetti, and E. Tognoni, "Measurement of Stark broadening of Mn I and Mn II spectral lines in plasmas used for laser-induced breakdown spectroscopy," Spectrochim. Acta B **62**, 1237–1245 (2007).
29. R. Rinaldi and X. Llovet, "Electron probe microanalysis: a review of the past, present, and future," Microsc. Microanal. **21**, 1053–1069 (2015).